Air-Liquid Interfaces of Aqueous Solutions Containing Ammonium and Sulfate: Spectroscopic and Molecular Dynamics Studies

*Sandhya Gopalakrishnan, Pavel Jungwirth,† Douglas J. Tobias,‡ Heather C. Allen**

Department of Chemistry, The Ohio State University, 100 W. 18th Ave., Columbus, Ohio 43210.

†Institute of Organic Chemistry and Biochemistry, Academy of Sciences of the Czech Republic and Center for Complex Molecular Systems and Biomolecules, Flemingovo nam. 2, 16610 Prague 6, Czech Republic, pavel.jungwirth@uochb.cas.cz

‡Department of Chemistry, University of California, Irvine, Irvine, CA 92697-2025

RECEIVED DATE (to be automatically inserted after your manuscript is accepted if required according to the journal that you are submitting your paper to)

*author to whom correspondence should be addressed, allen@chemistry.ohio-state.edu

Abstract

Investigations of the air-liquid interface of aqueous salt solutions containing ammonium (NH_4^+) and sulfate (SO_4^{2-}) ions were carried out using molecular dynamics simulations and vibrational sum frequency generation spectroscopy. The molecular dynamics simulations show that the predominant effect of SO_4^{2-} ions, which are strongly repelled from the surface, is to increase the thickness of the interfacial region. The vibrational spectra reported are in the O-H stretching region of liquid water. Isotropic Raman and ATR-FTIR (attenuated total reflection Fourier transform infrared) spectroscopies

were used to study the effect of ammonium and sulfate ions on the bulk structure of water; whereas surface sum frequency generation (SFG) spectroscopy was used to study the effect of these ions on the interfacial structure of water. Analysis of the interfacial and bulk vibrational spectra reveal that aqueous solutions containing SO_4^{2-} perturb the interfacial water structure differently than the bulk, and consistent with the molecular dynamics simulations, reveal an increase in the thickness of the interfacial region.

Introduction

It is well known that aerosols can affect the earth's climate directly by scattering and absorbing radiation, and indirectly by serving as cloud condensation nuclei (CCN), thereby modifying the optical properties and lifetime of clouds.[1-3] In order to develop accurate models to predict climate change, it is important to consider the optical properties, which are influenced by composition and growth of aerosols. The concentration of sulfuric acid in tropospheric aerosols is typically greater than 40 weight% and can be neutralized by gaseous ammonia to form NH_4HSO_4 and $(NH_4)_2SO_4$.[4] Several studies have shown that ammonium sulfate aerosols are abundant in the atmosphere;[5-8] Talbot *et al*. have measured comparable amounts of NH_4^+ and SO_4^{2-} in tropospheric aerosols.[9]

Sulfate aerosols are important in the context of aerosol transformation and growth. For example, ammonium sulfate aerosols play an important part in the heterogeneous hydrolysis of N_2O_5 to form nitric acid. A recent report by Kane *et al*.[10] shows that the uptake of N_2O_5 by $(NH_4)_2SO_4$ and NH_4HSO_4 aerosols is significant at relative humidity >50% showing that the process is governed by the presence of water in these aerosols. Kane *et al*. further postulate that the reaction primarily takes place with the water at the surface of the aerosol. However, the mechanism for this reaction is still unknown. Several recent studies have proposed that it is the interface that governs much of the chemistry in aerosols.[11-13] The above example hints that the hydrolysis of N_2O_5 can be catalyzed by the presence of interfacial water (as opposed to ammonium or sulfate). Knowledge of the molecular structure of the interface of aerosols can help to elucidate the reaction mechanism at the interface. The work described in this paper addresses fundamental issues regarding the interfacial molecular structure of aerosols containing ammonium and sulfate.

Surface tension measurements provide macroscopic information about the concentration changes (with respect to the bulk) in the surface region of aqueous salt solutions. Namely, the increase of surface tension of simple inorganic salt solutions compared to neat water is related via the Gibbs adsorption equation to a net decrease of ionic concentration in the interface. However, surface tension data provide only an integrated value of the ionic deficit over the whole interfacial region, which can be several molecular layers thick. In order to obtain more refined and detailed information about the distribution of ions at the air/water interface, in addition to conducting surface tension measurements, we have combined the surface selective technique of vibrational sum frequency generation (SFG) spectroscopy with molecular dynamics (MD) simulations of extended aqueous slabs containing molar concentrations of ammonium sulfate, sodium sulfate, and ammonium chloride.

Sum Frequency Generation Background

The theory of SFG has been described extensively in the literature.[14-18] Only a brief overview will be presented here. SFG is a second-order nonlinear process that occurs in non-centrosymmetric environments such as interfaces under the electric-dipole approximation. The SFG intensity, I_{SFG}, is shown in Eq. (1a),

$$I^{\omega_{SFG}}(\omega) \propto \left| E^{\omega_{SFG}} \cdot \chi^{(2)} : E^{\omega_{vis}} E^{\omega_{IR}} \right|^2 I^{\omega_{vis}} I^{\omega_{IR}} \qquad (1a)$$

where $I^{\omega_{SFG}}(\omega)$ is the intensity of the SFG and is a function of the frequency ω, $I^{\omega_{vis}} I^{\omega_{IR}}$ is the intensity of the incident visible multiplied by the incident IR, and $\left| E^{\omega_{SFG}} \cdot \chi^{(2)} : E^{\omega_{vis}} E^{\omega_{IR}} \right|^2$ is the absolute square of the E field at the interface denoted by superscripts that define the frequency of the exigent (SFG) and the incident (visible and IR) frequencies. E includes the Fresnel terms. $\chi^{(2)}$ is the tensor that describes the macroscopic susceptibility of the system. $\chi^{(2)}$ is expanded in Eq. (1b) to

$$\left| \chi^{(2)} \right|^2 = \left| \chi_{NR}^{(2)} + \sum_{\nu} \chi_{\nu}^{(2)} \right|^2 \qquad (1b).$$

The macroscopic second order susceptibility, $\chi^{(2)}$, consists of a non-resonant term ($\chi_{NR}^{(2)}$) and resonant terms ($\chi_v^{(2)}$). When the frequency of an incident infrared beam, ω_{IR} , is resonant with a vibrational mode of an interfacial molecule, *v*, the resonant susceptibility term $\chi_v^{(2)}$ dominates $\chi^{(2)}$ and a SFG intensity enhancement is observed. $\chi_v^{(2)}$ is given below in Eq. (2),

$$\chi_v^{(2)} \propto \frac{A_v}{\omega_v - \omega_{IR} - i\Gamma_v} \tag{2}$$

where A_v is the amplitude of the SFG transition moment, ω_v is the frequency of the transition and Γ_v describes the line-width of the transition. The amplitude, A_v, is nonzero when the Raman and the infrared transitions are spectroscopically allowed. The macroscopic nonlinear susceptibility $\chi^{(2)}$ is related to the molecular susceptibility, $\beta_{lmn,v}$. The molecular susceptibility can be described by Eq. (3),

$$\beta_{lmn,v} = \frac{\langle g|\alpha_{lm}|v\rangle\langle v|\mu_n|g\rangle}{\omega_{IR} - \omega_v + i\Gamma_v} \tag{3}$$

where $\langle g|\alpha_{lm}|v\rangle$ represents the Raman tensor for the transition, $\langle v|\mu_n|g\rangle$ represents the IR transition moment for the molecule and *lmn* represents the molecule fixed axes. An Euler angle transformation relates the laboratory coordinate system *(I,J,K)* to the molecular coordinate system *(l,m,n)*. The transformation is shown in Eq. (4)

$$\beta_{IJK,v} = \sum_{lmn} \mu_{IJK:lmn}\beta_{lmn,v} \tag{4}$$

where $\mu_{IJK:lmn}$ is the Euler angle transformation between the laboratory-coordinates *(I,J,K)* and the molecule-coordinates *(l,m,n)*. The macroscopic susceptibility, $\chi_{IJK,v}^{(2)}$, is therefore calculated from the molecular susceptibility, $\beta_{IJK,v}$, as shown in Eq. (5),

$$\chi^{(2)}_{IJK,\nu} = N\langle \beta_{IJK,\nu} \rangle \quad (5)$$

where $\chi_{IJK,\nu}$ is equal to the number density, N, multiplied by the ensemble average of $\beta_{IJK,\nu}$.

Recasting Eq. 5,

$$\chi^{(2)}{}_{IJK,\nu} = N \sum_{lmn} \langle \mu_{IJK:lmn} \rangle \beta_{lmn,\nu} = N \sum_{lmn} \langle \mu_{IJK:lmn} \rangle \frac{\langle g|\alpha_{lm}|\nu\rangle\langle\nu|\mu_n|g\rangle}{\omega_{IR} - \omega_\nu + i\Gamma_\nu} \quad (6)$$

For a single vibrational mode we can ignore phase; thus from Equations 1 and 6, we have

$$I^{\nu}_{SFG} \propto N^2 \left(\sum_{lmn} \langle \mu_{IJK:lmn} \rangle \left| \langle g|\alpha_{lm}|\nu\rangle\langle\nu|\mu_n|g\rangle \right| \right)^2 \quad (7)$$

Eq. 7 relates the SFG intensity to the Raman and IR tensors for the transition (the square of each tensor is the intensity) for a single vibrational mode.

Experimental

SFG Spectra

The air-liquid interface in the O-H stretching region of water (2800 – 3900 cm^{-1}) was probed using a scanning SFG system which has been described in detail elsewhere.[27] Essentially, the scanning SFG system uses a 532 nm frequency doubled output of a Nd:YAG laser (EKSPLA PL 2143 A/SS, 10 Hz repetition rate, 29 ps pulse duration) and an infrared beam from a KTP/KTA based optical parametric generator/amplifier (OPG/OPA, Laservision). The infrared beam is tunable from 2500-4000 cm^{-1} and has a bandwidth of ~8 cm^{-1}. The 532 nm beam is focused on the liquid surface using a plano-convex lens to yield a beam diameter of ~1 mm with a pulse energy of ~400 μJ. The IR beam is focused near the sample surface using a BaF_2 lens to yield a diameter of <0.5 mm. The peak IR energy (at ~3400 cm^{-1}) was ~400 μJ. The IR profile was measured simultaneously with the SFG spectrum by reflecting ~5% of the beam intensity onto an IR energy meter (Molectron-Coherent J9LP) using a BaF_2 window.

The input angles were ~48^{o} and ~57^{o} for the 532 nm and IR beams respectively from the surface normal. The detection angle was set to ~51^{o} from the surface normal for sum frequency. A 512 x 512 pixel thermoelectrically cooled back illuminated charge coupled device (CCD) (DV412, Andor Technology) was used to detect the sum frequency signal. A series of apertures were used to block the 532 nm (and IR) beam and only allow the sum frequency beam to be detected. In addition, a series of notch and short-pass optics were used to filter out the scattered 532 nm light.

The SFG spectra presented here were acquired using a 15 s exposure time per data point, leading to an acquisition time of ~30 minutes for the spectral range of 2800-3900 cm^{-1}. An average of 4 replicate spectra is presented in each case. Spectra of neat water were acquired at least once before and after each salt solution to confirm reproducibility. The polarization combination used for the SFG spectra was S, S, and P for sum frequency, visible, and IR respectively, where S polarization has its E field vector perpendicular to the incident plane and P polarization has its E field vector parallel to the incident plane. The SFG spectra were calibrated using the infrared absorption spectrum of a polystyrene film and the error in determining the absolute infrared frequency was ± 3 cm^{-1}.

It is desirable that the SFG spectra be normalized to take into account temporal and spatial overlap anomalies over the entire spectral region. Normalizing the SFG spectra to the sum frequency response from a GaAs crystal can do this. However, the infrared profile can change slightly from one spectrum to another and since we currently do not monitor the SFG from the GaAs crystal as well as the air-liquid interface simultaneously, the spectra shown in this paper were normalized to the IR profile. Spectra were also normalized to the GaAs crystal and found to be comparable to those normalized to the IR profile.

Raman Spectra

Raman spectra were obtained using unpolarized light and polarized light in separate studies conducted at ~24 ^{o}C. Unpolarized Raman spectra were acquired using a 532 nm continuous wave (CW) YAG laser (Spectra Physics, Millenia II), a 5 mm focusing Raman probe (InPhotonics, RP 532-05-15-FC), a

500 mm monochromator (Acton Research, SpectraPro SP-500) using a 1200 groove/mm grating, and a back illuminated CCD (Roper Scientific, LN400EB, 1340 x 400 pixel array and deep depletion). The collection fiber optic (which is part of the InPhotonics Raman probe) was coupled to the entrance slit of the monochromator. The power of the 532 nm beam was ~ 250 mW. The monochromator was calibrated using the 435.83 nm line from fluorescent light and was verified by comparison to the Raman spectrum of naphthalene.

Polarized Raman studies (isotropic and anisotropic) were completed by passing collimated (~1 mm diameter beam) vertically polarized light from the YAG laser (~200 mW) onto the sample and detecting the scatter with the Raman probe. A 90^{o} configuration for the incoming laser beam and detection was used. A sheet polarizer was placed between the sample and probe to select the polarization of the Raman scatter. The bandpass for all Raman experiments was ~ $3cm^{-1}$.

ATR-FTIR Spectra

ATR-FTIR spectra were obtained using a Thermo Nicolet spectrometer (Avatar 370, Thermo Electron Corporation). A 45^{o} single bounce ZnSe crystal trough mounted on an accessory (Smart SpeculATR) was used to collect spectra at a resolution of 4 cm^{-1} and averaged over 32 scans at ~24 ^{o}C.

Spectral Fits

The SFG spectrum, which is a plot of the SFG intensity (I_{SFG}) as a function of the incident infrared frequency (v), can be mathematically fit according to Eq. (1). When performing the fit, a constant complex number is used as the non-resonant term ($\chi_{NR}^{(2)}$) and the sign of the amplitude (A_v) is used to denote the phase of the photons of the vibrational mode from the interfacial molecules, which incorporates orientation and relative vibrational phases. Eq. (2) indicates the Lorentzian line shape in the SFG spectrum fitting. In Raman and IR spectroscopy, the intensity is the summation of the intensity of each vibration, while in SFG the intensity is proportional to the absolute square of the summation of the $\chi_{v}^{(2)}$ and $\chi_{NR}^{(2)}$ of each vibration as shown in Eq. (1). This leads to different spectral character for SFG spectra relative to Raman and IR spectra. Therefore, SFG spectral interpretation must occur after

deconvolution into the component peaks since direct comparison of SFG spectra to Raman and IR spectra may be misleading, in particular for the broad bands of the hydrogen bonding region (3000 – 3600 cm^{-1}).

All spectral fits shown in this paper were performed using the software package IGOR (version 4.0.5.1). For the Raman and ATR spectra, built-in algorithms were used to fit the spectra to Gaussian and Voigt line shapes respectively. In the case of the SFG spectra, a Lorentzian fitting function written to incorporate phase was invoked by IGOR to fit the spectra.

As shown in the Results and Discussion section, error bars are plotted for the deconvoluted peak areas for the Raman, ATR, as well as SFG spectra. The error bars were obtained as follows. For the Raman and ATR data, the error bars for the peak areas were computed by the fitting algorithm used by IGOR and appear in the output. In the case of the SFG data, the error bars were calculated by an entirely different method. Two sets of spectra were obtained of neat water and the salts over a period of several days. The error bars are the standard deviations obtained from the two independent fits.

Line Shapes

All Raman spectra were fit to pure Gaussians, ATR FTIR spectra were fit to a Voigt line shape and all SFG spectra were fit to pure Lorentzians. The spectral line shapes depend on line broadening mechanisms as well as instrumental factors. Homogeneous line broadening leads to a Lorentzian line shape while inhomogeneous line broadening leads to a Gaussian line shape. In general, both line-broadening mechanisms occur in liquids. The differences in lineshapes for the three different spectra are most likely due to instrumental factors.[28]

Surface Tension

Surface tensions were measured using a surface tensiometer using the Wilhelmy method (DeltaPi, Kibron Inc., Finland). Values are averages of four measurements conducted at 23 ^{o}C.

Chemicals

All the salts studied are available commercially. The salt solutions were made using Nanopure water (resistivity 18-18.2 MΩcm) and filtered using a carbon filter (Whatman Carbon-Cap) to remove organic impurities. The concentration of the salts was monitored via the sulfate and/or the ammonium bands using ATR-FTIR.

Computational Method

The salt solution bulk region between two interfacial layers was modelled using molecular dynamics (MD) simulation in a slab arrangement.[19] The slab geometry was realized by employing three-dimensional periodic boundary conditions with an elementary box extended in one dimension. Simulations were performed for three different 1.2 M aqueous salt solutions. In each case the unit box of a size of 3 x 3 x 10 nm contained 864 water molecules and either 36 NH_4^+ and 18 SO_4^{2-}, or 36 Na^+ and 18 SO_4^{2-}, or 18 NH_4^+ and 18 Cl^-. For the ammonium sulfate solution, we also performed simulations with the system size doubled, resulting in a thick slab with 1728 H_2O, 72 NH_4^+, and 36 SO_4^{2-} placed in a 3x3x19.2 nm unit box.

In all MD simulations a polarizable force field was employed. Namely, for water we used the POL3 potential,[20] sodium and chloride parameters were the same as in our previous studies,[21] and for ammonium a non-polarizable potential[22] was employed adding a polarizability of 1.34 $Å^3$ on the nitrogen atom. For sulfate we developed a polarizable potential recently.[23] Due to the large polarizability of SO_4^{2-}, simulations of its aqueous solutions suffer from the so called polarization catastrophe.[24] In order to circumvent this problem we, therefore, reduced the polarizability of each of sulfate oxygens to 1.4 $Å^3$ (i.e., by 20 %) (as done in our previous study[25]), rather than increasing the size of the dianion.[23] Calculations were performed using the molecular dynamics code Amber6. [26]

Results and Discussion

Surface Tension Measurements

The surface tension of aqueous salt solutions of 1M $(NH_4)_2SO_4$, 1M Na_2SO_4, 1M NH_4Cl, 2M NH_4Cl (to compare the results for the same number of ammonium ions in $(NH_4)_2SO_4$ and NH_4Cl) and neat

water were measured at 23^0C and are plotted in Fig. 1. The results show the expected increase in surface tension with increasing number of ions or ionic multiplicity (compare the surface tensions of $(NH_4)_2SO_4$ and Na_2SO_4 with that of 1M NH_4Cl) as well as with increasing solute concentration (as shown for 1M and 2M NH_4Cl). The surface tension of 1M NaCl is also plotted in red to illustrate that NH_4Cl and NaCl (which contain the same number of ions of the same multiplicity) show a similar increase in surface tension. The relatively large increase in surface tension of the sulfate solutions with respect to neat water and solutions of monovalent halides implies, via the Gibbs adsorption equation,[29] that their aqueous interfaces are practically devoid of ions.

Molecular Dynamics Simulations

The integrated depletion of ions from the surface layer deduced from surface tension measurements is also borne out from MD simulations, which provide a detailed picture of the full interfacial region with molecular resolution. Fig. 2 shows the density profile of water oxygens and of the individual ionic species across the slab for 1.2 M solutions of NH_4Cl, Na_2SO_4 and $(NH_4)_2SO_4$, along with snapshots from the simulations of each system. All these profiles were obtained by averaging the ion distributions over a nanosecond MD trajectory. All plotted values are averages over the two halves of the slab. The interface is defined by the concentration gradient of the different species and by the lack of an inversion center (and is hence SFG active) while the bulk is defined as the region where the concentrations are homogeneously mixed and has a macroscopic center of inversion.

Aqueous ammonium chloride (see Fig. 2a) behaves qualitatively similar to sodium chloride, which was investigated earlier.[30] Namely, the cations are repelled from the surface and chloride anions reside closer to the surface than ammonium ions. Quantitatively, NH_4^+ moves by about 1 Å closer to the surface than Na^+ and, consequently, the difference between the cationic and anionic density profiles in the interfacial region is smaller in aqueous NH_4Cl than in aqueous NaCl.

Fig. 2b, which depicts the ionic density profiles for aqueous sodium sulfate, demonstrates the dramatically different surface behavior of multiply charged ions. The electrostatic penalty of bringing

the sulfate dianion close to the surface is large, therefore, SO_4^{2-} solvates deeper in the interfacial region, leaving a roughly 7 Å thick anion-free surface layer. The sodium cations are inherently less "surface-phobic", however, at 1.2 M the ion-ion interactions are strong enough to move them also deeper into the interface. Nevertheless, the signal from sodium cations disappears slightly closer to the surface than that of the sulfate dianions.

The ionic density profiles of aqueous $(NH_4)_2SO_4$ are similar to those of Na_2SO_4, with strong repulsion of all the ions from the surface region. This indicates that it is primarily the sulfate dianion which dictates the ionic distribution (compare Figs. 2c and 2b). Nevertheless, we observe certain cationic specificity, namely ammonium ions penetrate slightly closer to the surface than sodium ions, a behavior that we already observed when chloride was the counter-anion. Also note that in both sulfate solutions the strong ion repulsion from the air/water interface results in an increased concentration of ions in the center of the slab, well above the nominal 1.2 M value. At these relatively high concentrations and due to the presence of multiply charged ions a certain degree of ion clustering is observed.

While for solutions of monovalent ions our slab is thick enough for the ionic density profiles to reach roughly constant values in the central region of the slab (see Fig. 2a), this is not completely true for the aqueous sulfate. We have, therefore, performed an additional simulation of 1.2 M ammonium sulfate in a slab with a doubled thickness, to test the convergence of the ionic surface behavior with system size. The results of this large simulation, depicted in Fig. 3, show that indeed the interfacial ionic profiles were semi-quantitatively converged already in the smaller slabs. Note, however, that even in the larger slabs the ionic densities do not quite level off. This demonstrates that the interfacial region with varying ionic densities is significantly thicker in aqueous solutions of multiply charged ions compared to those of monovalent ions.

Spectroscopy – Spectral Assignments

SFG spectra were taken of 1M $(NH_4)_2SO_4$, 1M Na_2SO_4, and 2M NH_4Cl to directly study the air-liquid interface and to test the MD simulations. The SFG spectrum, SSP polarizations, in the OH stretch

region (~2900-3900 cm^{-1}) of the air - neat water interface, isotropic Raman and ATR-FTIR spectra of neat water are shown in Figures 4(a-c) respectively along with their calculated fits including the component peaks. There are several published SFG spectra of the neat air-water interface.[31-35] The spectral features observed in our neat water surface SFG spectra are similar to previously published neat water SFG spectra.[31-35]

The broad peaks in the 3000 – 3600 cm^{-1} region contain two prominent bands in the SFG, the Raman, and IR spectra of neat water, and are positioned at ~3250 and ~3450 cm^{-1}. Generally following spectral assignments for ice [36], and considering the increase in disorder of a noncrystalline system, the 3250 cm^{-1} peak in the Raman (3253 cm^{-1}) and IR (3215 cm^{-1}) spectra is attributed to the vibrational modes from 4 oscillating dipoles of 4-coordinate hydrogen-bonded water molecules. These collective vibrations can be viewed as possessing symmetric character. In the SFG spectrum (peak at ~3200 cm^{-1}) of neat water, this peak is attributed predominantly to the 3-coordinate water molecules at the surface that are single proton donor – double proton acceptor (DAA),[37-40] with minimal if any contribution from 4-coordinate interfacial oscillating dipole modes. We assign the 3450 cm^{-1} peak in the Raman, IR, and the SFG to the more asymmetrically oscillating dipoles from 4-coordinate hydrogen-bonded water molecules. This spectral region can also be described as arising from 4-coordinate water molecules where one hydrogen is a poor hydrogen bond donor. The 3450 cm^{-1} peak dominates the SFG spectrum as revealed through deconvolution of the spectrum into the component peaks as shown in Fig. 4(a), which is consistent with recent water cluster IR studies.[37,39] The peak at ~3550 cm^{-1} in the SFG (~3550 cm^{-1}), Raman (3630 cm^{-1}), and IR (3571 cm^{-1}) spectra[41,42] is assigned to the modes associated with 3-coordinate asymmetrically hydrogen-bonded water molecules in which one O-H bond is involved in strong hydrogen-bonding and the other is only weakly hydrogen-bonded.[41] For the SFG, these 3-coordinate species are double proton donor – single proton acceptor (DDA) molecules. [37-40] The narrow peak at 3700 cm^{-1} in the SFG spectrum of Fig. 4(a) is assigned to the dangling OH (surface free OH) stretch of water molecules that straddle the interface with one non-hydrogen bonded OH directed into the air phase[31,33,34] and the other OH interacting through hydrogen bonding with the liquid phase as described above within the ~3250

cm^{-1} SFG peak assignment.[38-40] The assignment of the component peak at ~3750 cm^{-1} in the SFG spectrum of neat water is still under debate; however, recent discussions [43] point to frustrated rotations of surface water molecules that are hydrogen-bonded via the oxygen (single and double acceptor-only water molecules). In summary, for the SFG, Raman, and IR spectral assignments of neat water, as the frequency increases, the hydrogen-bonding strength decreases and the asymmetric character of the modes increases.

SFG spectra were acquired from the air-aqueous ammonium sulfate interface as shown in Fig. 5. Comparison of the SFG spectra of neat water and aq. $(NH_4)_2SO_4$ clearly show different spectral intensities. There is a significant increase in intensity within the hydrogen-bonding region (2800-3600 cm^{-1}) of the aq. $(NH_4)_2SO_4$ relative to that of neat water. In order to interpret the SFG spectrum of aq. $(NH_4)_2SO_4$, a study of aqueous solutions of NH_4Cl and Na_2SO_4 was conducted to determine how individual ions affect the hydrogen bonding network of water. Raman, IR, and SFG spectra of all salt solutions were obtained to elucidate spectral assignments and interpretation.

The isotropic Raman spectra of the salt solutions in the water O-H stretch region are shown in Fig. 6a. Spectral assignments were made after deconvoluting the spectra into component peaks as shown in Figs. 6(b-e). In the case of aq. Na_2SO_4 (Fig. 6d), the spectral region between 2800 and 3800 cm^{-1} is essentially that from water since there are no bands from SO_4^{2-} or HSO_4^- in this region. The spectra are assigned as discussed above in the neat water assignments. In the case of aq. $(NH_4)_2SO_4$ (Fig. 4e) and NH_4Cl (Fig. 4c) however, the isotropic Raman spectra show that this spectral region can be complicated by NH_4^+ bands.[44] Spectra of 2M NH_4Cl were obtained in order to compare the affect of the same number of NH_4^+ ions on the structure of water in aq. $(NH_4)_2SO_4$ and NH_4Cl. The peak positions and assignments of vibrational bands previously observed in Raman and infrared spectra of aqueous ammonium sulfate of composition $(NH_4)_2SO_4.11H_2O$ [44] are given in Table 1. These were used as a guide to fit the spectra of the salt solutions. In the case of the ammonium salts, two additional peaks (other than the water peaks) assigned to the second overtone of the NH_4^+ umbrella bend (at ~2880 cm^{-1}) and a combination band of the NH_4^+ umbrella bending and rocking vibrations (at ~3035 cm^{-1}) are

observed in our Raman spectra and are in agreement with the Raman study of Spinner.[44] The peak positions, amplitudes, full width at half maximum (FWHM), and peak areas for the Raman spectra are collected in Table 2.

Deconvolution of the NH_4^+ bands in the 3000-3500 cm^{-1} region is non-trivial. In addition to the two bending modes, there are two fundamental vibrational modes involving the NH_4^+ stretch observed by Spinner; a symmetric stretch in aqueous ammonium sulfate of composition $(NH_4)_2SO_4.11H_2O$ at 3115 cm^{-1} and an asymmetric stretch assigned at 3215 cm^{-1}.[44] In the Raman studies conducted on even a solution of this high a concentration, the spectral depolarization ratios of both peaks could not be measured because of the overlap with the water O-H stretch as well as the 3060 cm^{-1} NH_4^+ combination band (see Table 1). In the case of a 1 M solution of $(NH_4)_2SO_4$, the 3100 - 3200 cm^{-1} region is overwhelmed by the water O-H stretch and thus these peaks could not be fit.

The ATR-IR spectra of the salt solutions in the water O-H stretch region are shown in Fig. 7a. As in the case of the Raman spectra, the IR spectrum of aq. Na_2SO_4 (Fig. 7d) in this region can be assigned to the vibrational modes from the hydrogen bonding network from water. Again, these assignments were made after deconvoluting the spectrum into component peaks as shown in Fig. 7d. In the case of the aq. ammonium salts, three additional peaks (other than the water peaks) were fit to the spectra as shown in Figs. 7c and 7e for aq. NH_4Cl and $(NH_4)_2SO_4$ respectively. These peaks at ~2880, 3060, and 3200 cm^{-1} were assigned (using previously observed IR band frequencies shown in Table 1 as a guide) to the 2nd overtone of the NH_4^+ umbrella bend, the combination band of the NH_4^+ umbrella bending and rocking vibrations, and the asymmetric NH_4^+ stretch respectively. The peak positions, amplitudes, FWHM, and peak areas for the ATR-IR spectra are collected in Table 3.

The SFG, SSP polarized, spectra of the salt solutions are shown in Fig. 8a. The average of 4 SFG spectra for each species is plotted. All the peaks in the spectral region 2800-3900 cm^{-1} for the aqueous salt solutions are assigned to the air-water interfacial O-H stretching modes as discussed above for the SFG spectrum of neat water. However, the 3250 cm^{-1} peak intensity increases for the sodium and

ammonium sulfate solutions are attributed to vibrational modes of the 4 oscillating dipoles of interfacial 4-coordinate water-oxygens. In the case of Na_2SO_4 (Fig. 8d), the assignments are quite unambiguous; however, in the case of the ammonium salts, the NH_4^+ bands observed in the Raman (at ~2880 and ~3040 cm^{-1}) and ATR-IR spectra (at ~2880, ~3060, and ~3200 cm^{-1}) introduce a complication because they overlap with the O-H stretching region of water. The 2880 and 3060 cm^{-1} peaks are weak in both the Raman and ATR-IR spectra and thus are expected to be weak in the SFG spectra as well (since the SFG intensity is proportional to the product of the Raman and IR transition moments, as per Eq. 7). The NH_4^+ stretch vibrations could not be assigned in the Raman spectra as mentioned before; thus their assignment in the SFG spectra would be highly ambiguous and was not incorporated in the spectral fits (although given the broadness and lower signal-to-noise ratio of the SFG spectra compared to Raman and IR spectra, additional peaks can be force fitted). The spectral fits of the SFG spectra after deconvolution into component peaks are shown in Fig. 8(b-e) with the corresponding spectral parameters given in Table 4.

Spectroscopy and Molecular Dynamics Simulations - Discussion

The intensity of the ~3250 cm^{-1} peak from the salt solutions relative to that of neat water from the SFG spectra is shown in Fig. 9a. The corresponding isotropic Raman x IR intensities are plotted for comparison with the SSP polarized SFG intensities (recall that the SFG intensity is proportional to the square of the product of the Raman and IR transition moments as well as the square of the number density (N), as per Eq. 7). The Raman x IR intensities show that the intensity of the 3250 cm^{-1} peak decreases to a small extent for all the salt solutions as compared to water, generally driven by the cation and anion replacing water molecules in the sampling volume consistent with the Raman results in Fig. 6a. However, in the SFG spectra the intensity of the ~3250 cm^{-1} peak increases in the order: $H_2O \approx 2M$ $NH_4Cl < 1M$ $Na_2SO_4 < 1M$ $(NH_4)_2SO_4$. An increase in the Raman and IR transition moment in the salts as compared to water can be ruled out since the product of the Raman and IR intensities actually decreases in the 3250 cm^{-1} peak (the product of the Raman and IR intensity is proportional to the product of the square of the respective transition moments). In addition to an increase in intensity in the

3250 cm^{-1} peak, there is also an increase in intensity in the 3450 cm^{-1} peak in aq. Na_2SO_4 and $(NH_4)_2SO_4$ which is shown in Fig. 9b. Similar to the analysis of the 3250 cm^{-1} band, an increase in the Raman x IR transition moments of the 3450 cm^{-1} band in the salt solutions as compared to neat water is ruled out as the full cause since the SFG intensity enhancement in Na_2SO_4 and $(NH_4)_2SO_4$ spectra is much larger than the Raman x IR enhancement.

Another explanation for the enhancement of the 3250 cm^{-1} and 3450 cm^{-1} bands in the SFG spectra of Fig. 8 (d-e) could be an increased ordering of the interfacial water molecules under the influence of a local weak electric field induced by the sulfate dianions in aq. Na_2SO_4 and $(NH_4)_2SO_4$ and/or an increase in the interfacial depth. (Recall that the SFG intensity is proportional to the square of the number density (N), as per Eq. 7, and that the intensities from the SSP polarized SFG spectra increase if the water molecules are better aligned with their transition moments normal to the surface; yet cancellation will occur if the vectors oppose each other.) The local weak electric field effect excludes the solvation shell water molecules that partially contribute to the 3450 cm^{-1} band of the salt solutions, although these molecules will minimally contribute with increasing interfacial depth. The above explanation is consistent with the MD simulations on the aqueous solutions of NH_4Cl, Na_2SO_4, and $(NH_4)_2SO_4$ shown in Figs 2(a-c) and Fig. 3, as discussed above.

To further explore the localized field effect, we turn to the MD simulations. Since the SFG contribution from molecules in centrosymmetric environments vanishes, the inhomogeneous interfacial region probed by the SFG experiments is better defined in terms of the region over which there is a net orientational polarization of water molecules. To this end, in Fig. 10 we have plotted $\langle cos\theta \rangle$, as a function of location in slabs of neat water and two ammonium salts, 1.2 M NH_4Cl (i.e., salt with a monovalent anion), and 1.2 M $(NH_4)_2SO_4$ (i.e., a representative of a salt with a divalent anion). Here, θ is the angle between a water dipole moment and a vector normal to the slab surface (i.e. the *z* axis in the simulation cell), and the angular brackets denote an average over time and molecules. This quantity vanishes for an isotropic distribution of water orientations, and is nonzero where there is a net orientation of water dipoles. The orientational polarization and other quantities reported in Fig. 10 for

$(NH_4)_2SO_{4(aq)}$ were obtained from the simulation of the thicker system only because data obtained for the smaller system appeared to contain finite size artifacts.

The data plotted in Fig. 10 show that the interface, defined by nonzero values of $\langle cos\theta \rangle$, increases in width in the order H_2O < $NH_4Cl_{(aq)}$ < $(NH_4)_2SO_{4(aq)}$. The maximum degree of water orientational polarization is roughly the same in neat water and $(NH_4)_2SO_{4(aq)}$, and roughly twice that of $NH_4Cl_{(aq)}$. In neat water the orientational ordering is confined mostly to the surface layer, while in the NH_4Cl solution there appears to be an ordered subsurface layer about 10 Å below the Gibbs dividing surface in addition to an ordered surface layer. The orientational polarization decays slowly into the $(NH_4)_2SO_4$ solution, such that the width of the region over which water molecules have an appreciable net orientation is approximately 20 Å. This is consistent with the increase in SFG intensity of the 3000 – 3600 cm^{-1} region for the $(NH_4)_2SO_4$ (Fig 5 and Fig. 8a and e).

The thickening of the interface can contribute to the increase in the SFG intensity in the 3250 and the 3450 cm^{-1} regions from the sulfate solutions. It is not possible to distinguish between SFG signal enhancement due to ordering of water molecules under the presence of a weak electrostatic field and an increase in interfacial depth. However, the thickening of the interface is supported by orientation polarizations (Fig. 10), and density profiles (Fig. 2(b-c), Fig. 3) which reveal that the interfacial depth increases in aq. Na_2SO_4 and $(NH_4)_2SO_4$ (the density gradient extends over a larger region) as compared to aq. NH_4Cl (Fig. 2a). The interface is defined by the concentration gradient of the different species and lacks an inversion center (and is hence SFG active), while the bulk is defined as the region where the species are homogeneously mixed and therefore has a macroscopic center of inversion (and is hence SFG inactive). Thus, we conclude that the air-aqueous interface of the ammonium sulfate solution (as well as the sodium sulfate solution) has widened, and that local field effects caused by the sulfate dianions play a significant role in this interfacial behavior of water. These effects thereby account for the larger 3250 and the 3450 cm^{-1} peak intensities observed in the aq. $(NH_4)_2SO_4$ and the Na_2SO_4 SFG spectra (Figs 8 and 9).

To gain further insight into the SFG spectra, in addition to knowing the extent of structural inhomogeneity, it is also relevant to quantify the populations of water OH bonds in various settings. To this end, the water molecules are divided into three general groups: (1) those for which both OH bonds are hydrogen bond donors (2D) to other water molecules, (2) one OH bond is free and one is involved in a hydrogen bond with another water molecule (1D), and (3) both OH are free, i.e. not involved in any hydrogen bonds (0D). Water molecules involved in ion-water hydrogen bonds were excluded to simplify the analysis, and because they make a relatively insignificant contribution to the SFG spectra at the concentrations considered here. The surface density (number per unit area) of 2D, 1D, and 0D water molecules is shown as a function of position in the slabs in Fig. 11a-c, respectively. A geometric criterion was used to define hydrogen bonds: acceptor oxygen to donor hydrogen distance less than 3.5 Å, 3.8 Å, and 3.5 Å for water-water, water-chloride, and water-sulfate oxygen hydrogen bonds, respectively, and the acceptor O…O–H angle less than 30˚. In Fig. 11 (a-c) it is evident that the populations of the three OH species show qualitatively similar variations with position relative to the surface in all three solutions, in contrast to the orientational polarization profiles (Fig. 10).

The population of 2D water molecules increases rapidly on passing from the surface to the interior of all three systems (Fig. 11a), roughly tracking the water oxygen density profiles (Figs. 2 and 3). The population is reduced in the salt solutions compared to neat water, reflecting the replacement of water-water hydrogen bonds by ion-water hydrogen bonds.

The population of the 1D water molecules exhibits a peak in the interfacial layer and decays rapidly to a nearly constant value in the interior of the solutions (Fig. 11b). The overall number of 1D waters is slightly larger throughout in neat water than in the salt solutions, again because in the salt solutions some water-water hydrogen bonds are replaced by ion-water hydrogen bonds. There are slightly more 1D waters in the surface layer of $(NH_4)_2SO_{4(aq)}$ compared to $NH_4Cl_{(aq)}$, while in the interior of the solutions there are slightly more 1D waters in $NH_4Cl_{(aq)}$.

The populations of 0D water molecules (those with two free OH bonds) are very similar in all three systems throughout the slabs. Note that the number of water molecules with one free OH bond (1D) is about an order of magnitude greater than the number with two free OH bonds (0D). Overall, the total number of free OH bonds is similar in the three systems, and this is consistent with the nearly constant intensity in the free OH region (3700 cm^{-1} peak) of the SFG spectra.

In summary, no significant differences between neat water and the salt solutions are observed for the 2D, 1D, or the 0D surface densities. This suggests that the interpretation of the SFG spectral differences rests on differences in water orientational order. Recall that water molecules will only contribute to the SFG signal if they are in a noncentrosymmetric environment. Indeed, the greater intensity in the hydrogen bonded region of the SFG spectra for $(NH_4)_2SO_{4(aq)}$ versus $NH_4Cl_{(aq)}$ and neat water reflects the longer range of orientational ordering (i.e. thicker interfacial region) as shown in Fig. 10.

Conclusions

The air-liquid interface of aqueous solutions containing ammonium and sulfate ions (NH_4Cl, Na_2SO_4, and $(NH_4)_2SO_4$) was investigated using molecular dynamics simulations and using vibrational sum frequency generation spectroscopy in the O-H stretching region of liquid water. Our SFG results show, after comparison to isotropic Raman and ATR-FTIR spectra, enhanced intensity in the water O-H vibrational modes at the air-liquid interface in aq. $(NH_4)_2SO_4$ and Na_2SO_4 compared to aq. NH_4Cl, and neat water. In the case of aq. NH_4Cl, the perturbation of the hydrogen-bonded network of water due to the ions is similar at the interface and the bulk. Furthermore, comparison of interfacial and bulk vibrational structure reveals differences at the air-liquid interface relative to the bulk by ions in aq. $(NH_4)_2SO_4$ and Na_2SO_4. The molecular dynamics simulations combined with the SFG results reveal a thickening (widening) of the air-liquid interface for the aq. sulfate solutions, which is inclusive of alignment of the interfacial water molecules extending deeper into the bulk solution.

Acknowledgement

Support from the US-NSF (grant CHE-0209719), NSF-CAREER (grant CHE-0134131), and from the Czech ministry of education (grant ME644) is gratefully acknowledged. Part of the work in Prague was completed within the framework of research project Z40550506. The authors gratefully acknowledge V. Buch, P. Devlin, and U. Buck for extensive discussions of this work. We also thank D. Liu for assistance.

References

(1) Anderson, T. L.; Charlson, A. J.; Schwartz, S. E.; Knutti, R.; Boucher, O.; Rodhe, H.; Heintzenberg, J. *Science* **2003**, *300*, 1103.

(2) Crowley, T. J. *Science* **2000**, *289*, 270.

(3) *Climate Change 2001: The Scientific Basis*; Houghton, J. T.; Ding, Y.; Griggs, D. J.; Noguer, M.; Linden, P. J. V. d.; Dai, X.; Maskell, K.; Johnson, C. A., Eds., 2001.

(4) Keene, W. C.; Sander, R.; Pszenny, A. A. P.; Vogt, R.; Crutzen, P. J.; Galloway, J. N. *J. Aerosol Sci.* **1998**, *29*, 339.

(5) Posfai, M.; Anderson, J. R.; Buseck, P. R.; Shattuck, T. W.; Tindale, N. W. *Atmos. Environ.* **1994**, *28*, 1747.

(6) Chelf, J. H.; Martin, S. T. *J. Geophys. Res. - Atmos.* **2001**, *106*, 1215.

(7) Prenni, A. J.; Wise, M. E.; Brooks, S. D.; Tolbert, M. A. *J. Geophys. Res. - Atmos.* **2001**, *106*, 3037.

(8) Sander, R.; Lilieveld, J.; Crutzen, P. J. *J. Atmos. Chem.* **1995**, *20*, 89.

(9) Talbot, R. W.; Dibb, J. E.; Loomis, M. B. *Geophys. Res. Lett.* **1998**, *35*, 1367.

(10) Kane, S. M.; Caloz, F.; Leu, M. *J. Phys. Chem. A* **2001**, *105*, 6465.

(11) Donaldson, D. J.; Guest, J. A.; Goh, M. C. *J. Phys. Chem.* **1995**, *99*, 9313.

(12) Finlayson-Pitts, B. J.; Pitts, J. N. *Chemistry of the Upper and Lower Troposphere*; Academic Press:, 2000.

(13) Longfellow, C. A.; Imamura, T.; Ravishankara, A. R.; Hanson, D. R. *J. Phys. Chem. A* **1998**, *102*, 3323.

(14) Shen, Y. R. *The principles of nonlinear optics*, 1st ed.; John Wiley & Sons: New York, 1984.

(15) Bloembergen, N.; Pershan, P. S. *Phys. Rev.* **1962**, *128*, 606.

(16) Miranda, P. B.; Shen, Y. R. *J. Phys. Chem. B* **1999**, *103*, 3292.

(17) Hirose, C.; Akamatsu, N.; Domen, K. *Appl. Spectrosc.* **1992**, *46*, 1051.

(18) Moad, A. J.; Simpson, G. J. *J. Phys. Chem.* **2004**, *108*, 3548.

(19) Wilson, M. A., Pohorille. *J. Chem. Phys.* **1991**, *95*, 6005.

(20) Caldwell, J. W.; Kollman, P. A. *J. Phys. Chem.* **1995**, *99*, 6208.

(21) Jungwirth, P.; Tobias, D. J. *J. Phys. Chem. B* **2002**, *106*, 6361.

(22) Boudon, S., Wipff, G. J. *J. Comp. Chem.* **1991**, *12*, 42.

(23) Jungwirth, P.; Curtis, J. E.; Tobias, D. J. *Chem. Phys. Lett.* **2003**, *367*, 704.

(24) Thole, B. T. *Chem. Phys.* **1981**, *59*, 341.

(25) Jungwirth, P.; Rosenfeld, D.; Buch, V. *Atmos. Res.*,, In Press.

(26) Case, D. A.; Pearlman, D. A.; Caldwell, J. W.; Cheatham III, T. E., Ross, W. S.; Simmerling, C. L.; Darden, T. A.; Merz, K. M.; Stanton, R. V.; Cheng, A. L.; Vincent, J. J.; Crowley, M.; Tsui, V.; Radmer, R. J.; Duan, Y.; Pitera, J.; Massova, I.; Seibel, G. L.; Singh, U. C.; Weiner, P. K.; Kollman, P. A. Amber 6; University of California: San Francisco, 1999.

(27) Liu, D.; Ma, G.; Levering, L. M.; Allen, H. C. *J. Phys. Chem. B* **2004**, *108*, 2252.

(28) Stewart, J. E. *Infrared Spectroscopy - Experimental Methods and Techniques*; Marcel Dekker Inc.:, 1970.

(29) Gibbs, J. W. *The Collected Works of J. W. Gibbs*; Longmans: New York, 1931; Vol. 1.

(30) Jungwirth, P.; Tobias, D. J. *J. Phys. Chem. B* **2001**, *105*, 10468.

(31) Allen, H. C.; Raymond, E. A.; Richmond, G. L. *J. Phys. Chem.* **2001**, *105*, 1649.

(32) Shultz, M. J.; Baldelli, S.; Schnitzer, C.; Simonelli, D. *J. Phys. Chem. B* **2002**, *106*, 5313.

(33) Du, Q.; Superfine, R.; Freysz, E.; Shen, Y. R. *Phys. Rev. Lett.* **1993**, *70*, 2313.

(34) Schnitzer, C.; Baldelli, S.; Campbell, D. J.; Shultz, M. J. *J. Phys. Chem. A* **1999**, *103*, 6383.

(35) Allen, H. C.; Raymond, E. A.; Richmond, G. L. *Current Opinion in Colloid & Interface Science* **2000**, *5*, 74.

(36) Buch, V., Devlin, J. P. *J. Chem. Phys.* **1999**, *110*, 3437.

(37) Brudermann, J.; Melzer, M.; Buck, U.; Kazimirski, J. K.; Sadlej, J.; Buch, V. *J. Chem. Phys.* **1999**, *110*, 10649.

(38) Buck, U.; Ettischer, I.; Melzer, M.; Buch, V.; Sadlej, J. *Phys. Rev. Lett.* **1998**, *80*, 2578.

(39) Devlin, J. P.; Sadlej, J.; Buch, V. *J. Phy. Chem. A* **2001**, *105*, 974.

(40) Pribble, R. N.; Zwier, T. S. *Science* **1994**, *265*, 75.

(41) Scherer, J. R. Chapter 3. The vibrational spectroscopy of water. In *Advances in Infrared and Raman Spectroscopy*; Clark, R. J. H., Hester, R. E., Eds.; Heyden: Philadelphia, 1978; Vol. 5; pp 149.

(42) Scherer, J. R.; Go, M. K.; Kint, S. *J. Phys. Chem.* **1973**, *77*, 2108.

(43) Shultz, M. J., Private Communication.

(44) Spinner, E. *Spectrochimica Acta Part A* **2003**, *59*, 1441.

List of Figures

List of Tables

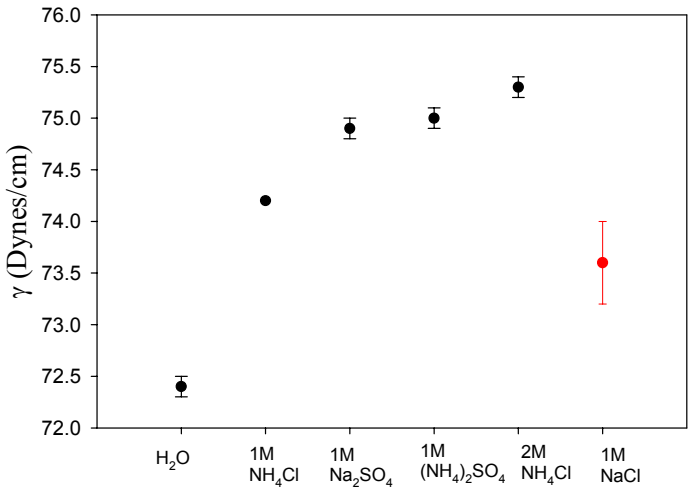

Figure 1. Plot of the surface tension of the aqueous salt solutions at 23^0C.

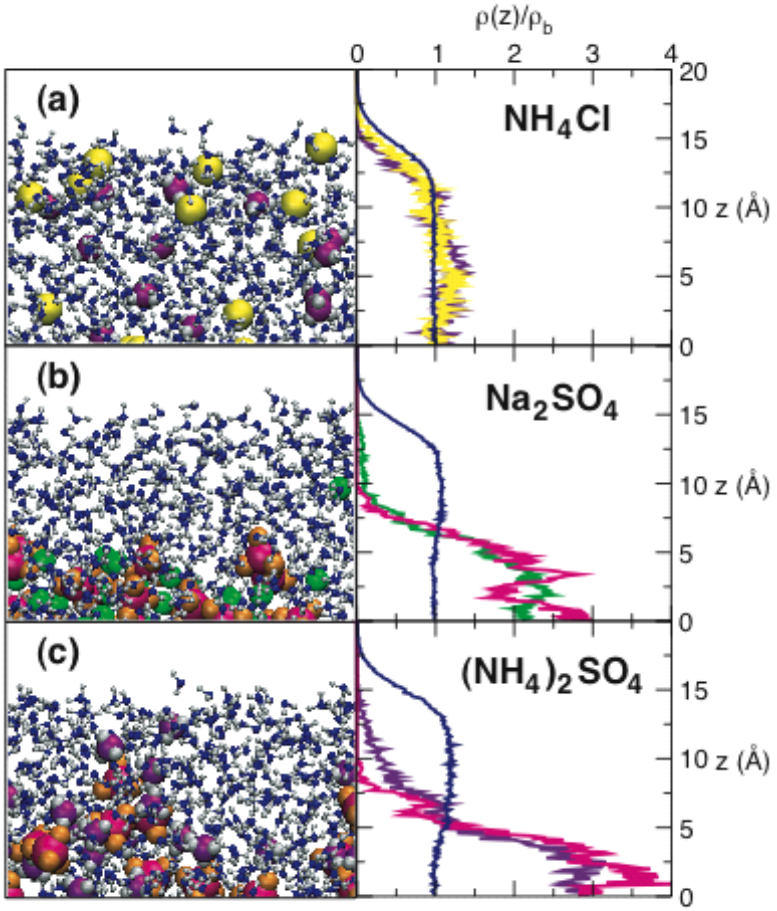

Figure 2. Left panels: snapshot from MD simulations of 1.2 M aqueous solutions of (a) ammonium chloride; (b) sodium sulfate; (c) ammonium sulfate. Right panels: corresponding density profiles of salt ions and water oxygens from the center of the slab (z = 0) to the air/water interface. Coloring scheme: H, gray; water O, blue; chloride, yellow; sodium, green; ammonium N, purple; sulfate S, magenta; sulfate O, orange.

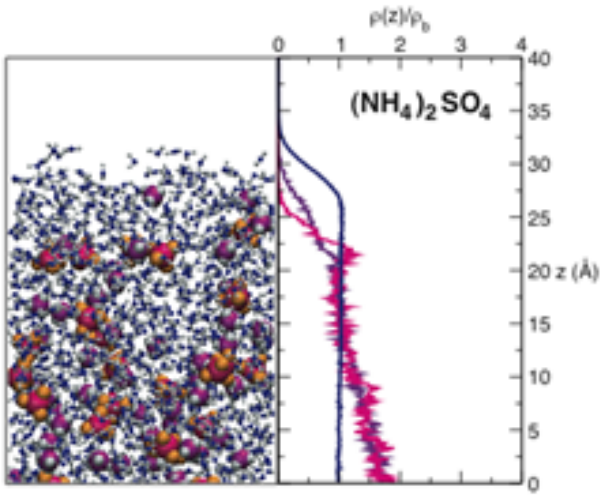

Figure 3. Left panel: snapshot from an MD simulation of a 1.2 M aqueous solution of sodium sulfate for a slab with doubled thickness and, consequently, doubled number of atoms as compared to Fig. 2c. Right panel: corresponding density profiles. The coloring scheme is the same as in Fig. 2.

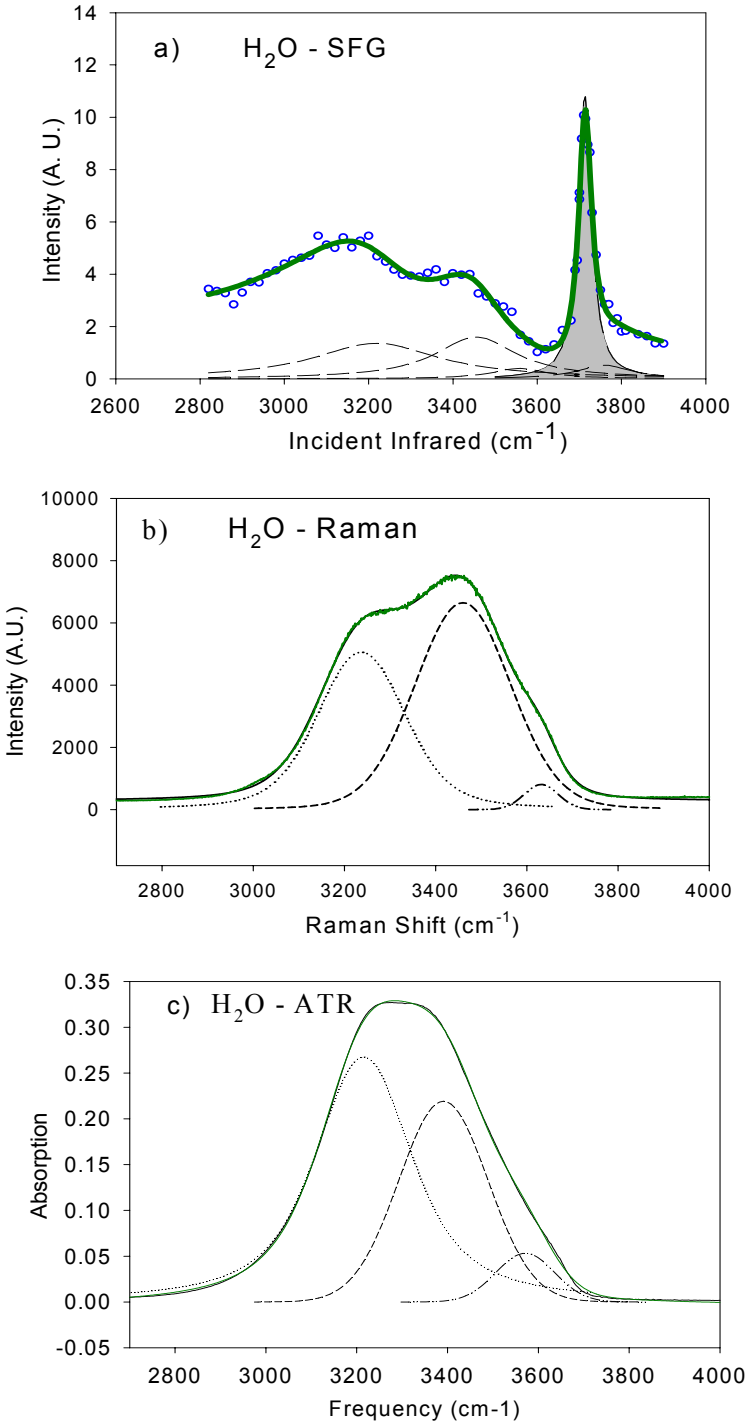

Figure 4. a) SFG SSP-polarized spectrum of neat water in the O-H stretching region (the deconvoluted peaks shaded in gray have "-" phase while those which are not shaded have "+" phase), the component peak at ~3550 cm^{-1} is multiplied by 20, b) Isotropic Raman spectrum of neat water, c) ATR-IR spectrum of neat water. The calculated spectra from the spectral fits are shown in green.

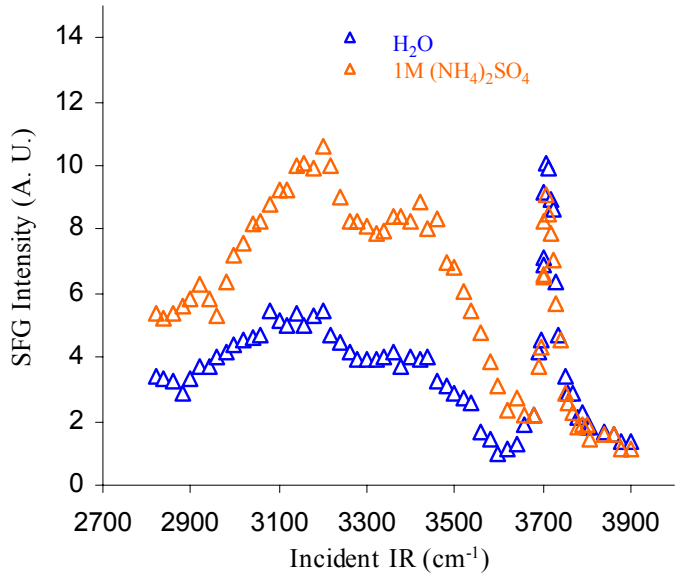

Figure 5. SFG SSP-polarized spectrum of 1M aqueous ammonium sulfate compared to that of neat water.

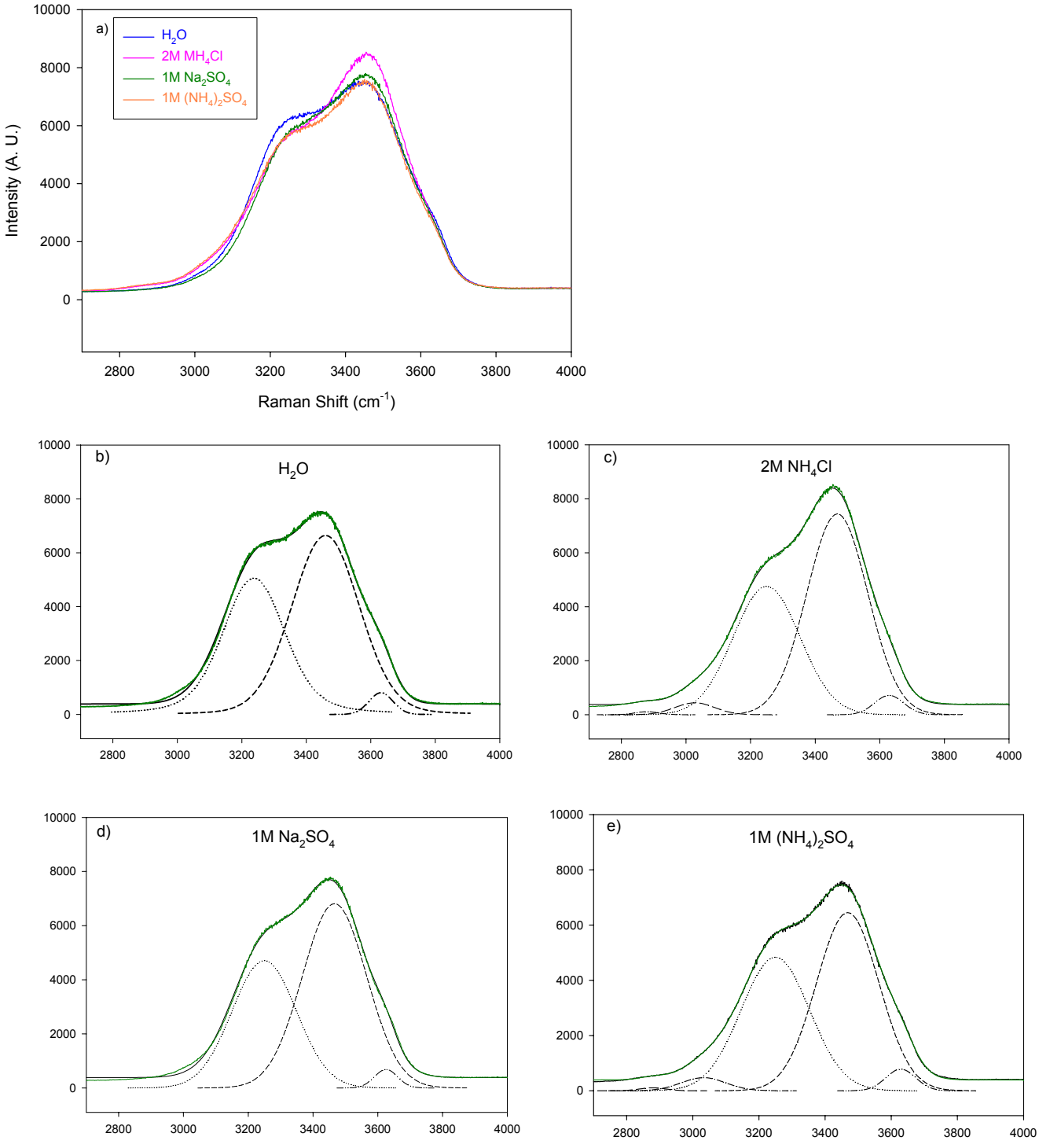

Figure 6. a) Isotropic Raman spectra of various salt solutions compared to that of neat water, (b-e) spectral fits of Raman spectra. The fitted spectral profile is shown in green.

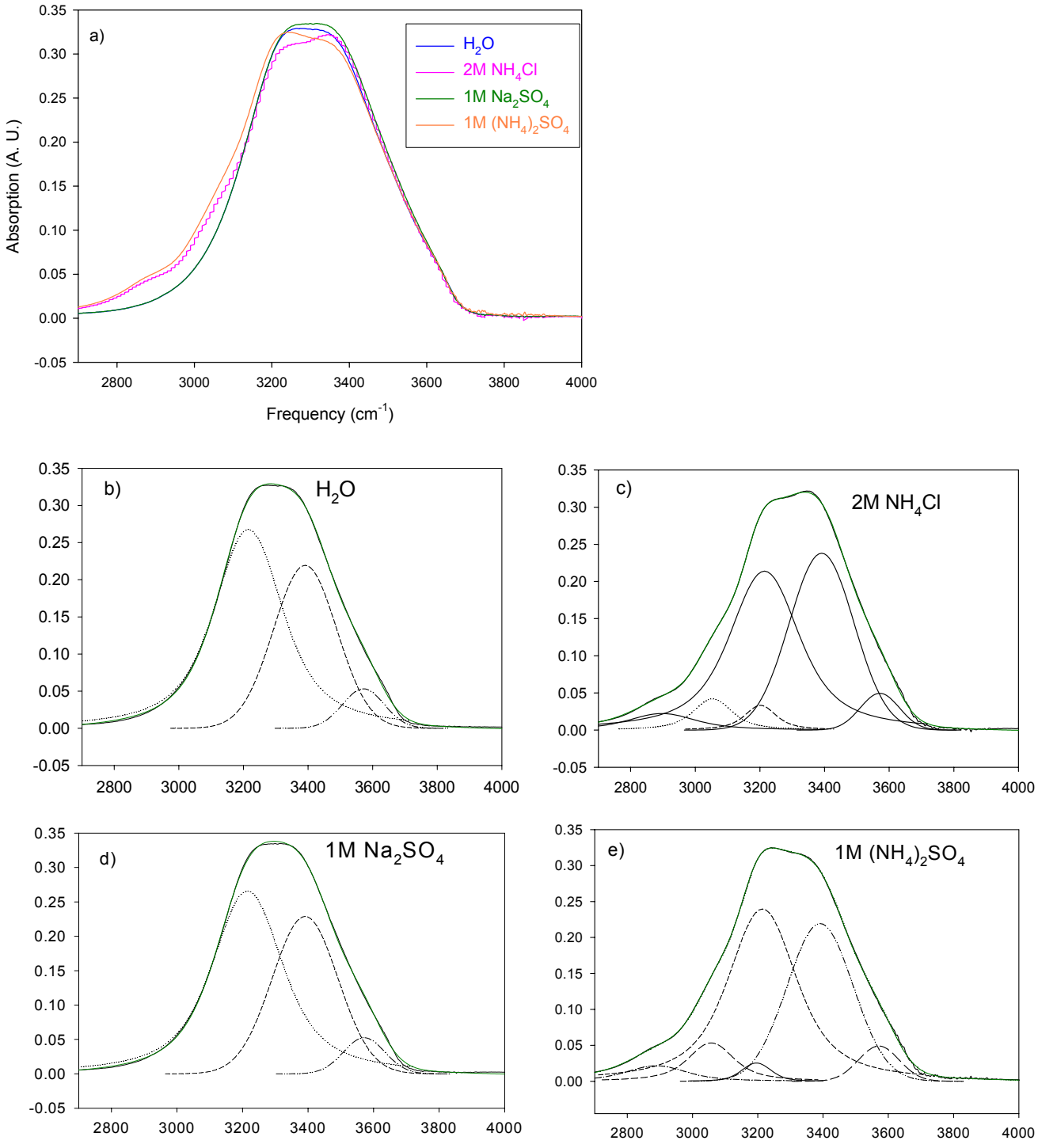

Figure 7. a) FTIR-ATR spectra of various salt solutions compared to that of neat water, (b-e) spectral fits of ATR spectra. The fitted spectral profile is shown in green.

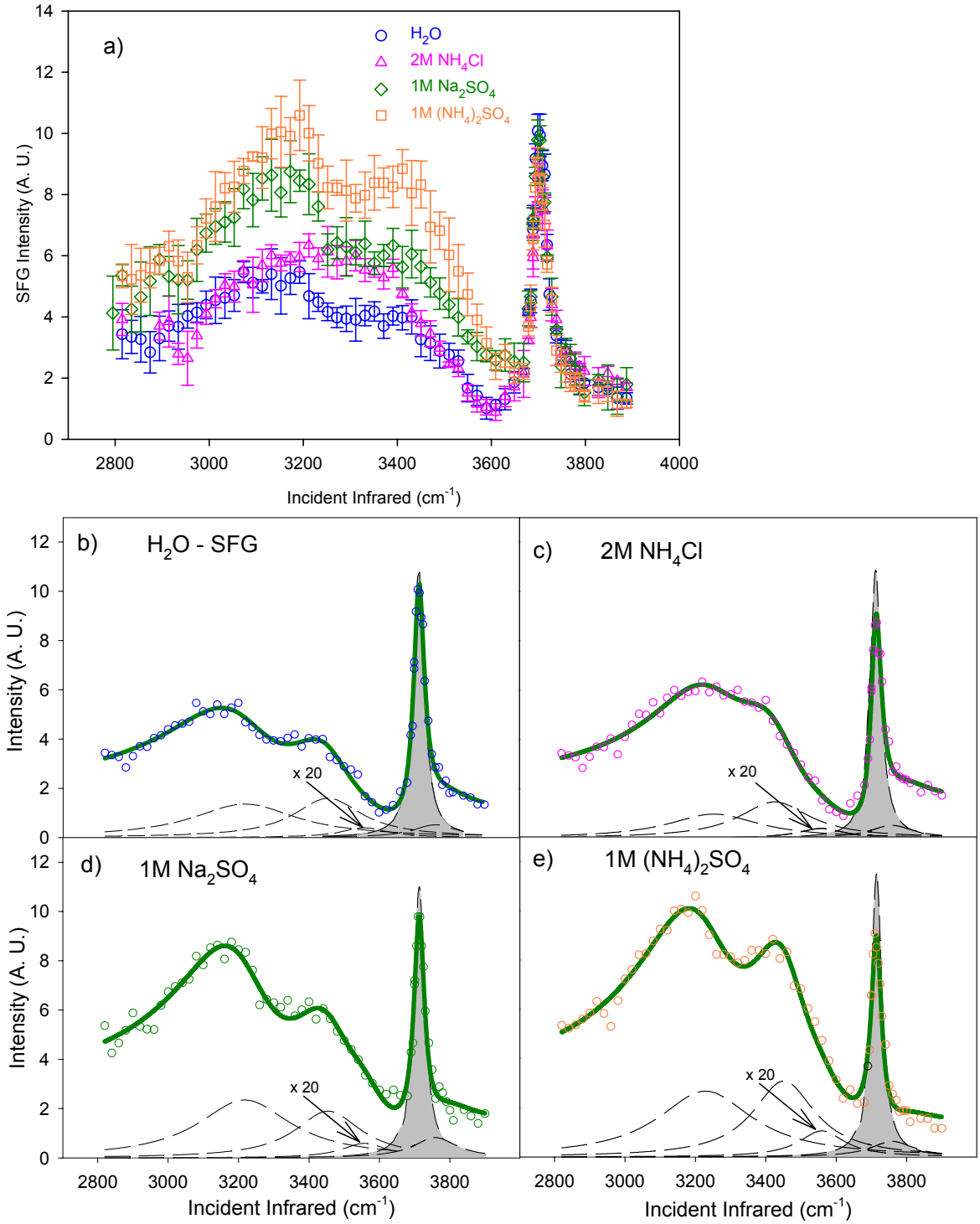

Figure 8. a) SFG SSP-polarized spectra of various salt solutions compared to that of neat water, (b-e) spectral fits of SFG spectra. The green solid line shows the fitted spectral profile. The component peaks shaded in gray have "-" phase while those which are not shaded have "+" phase.

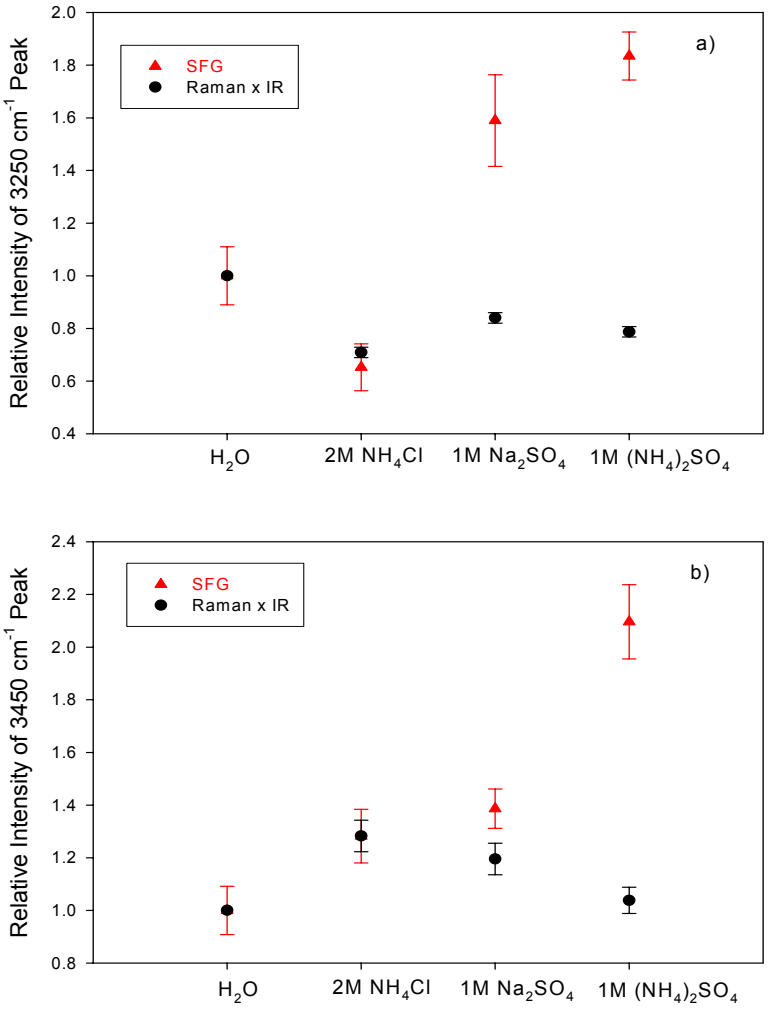

Figure 9. a) Plot of the relative (to water) intensities of the 3250 cm^{-1} peak. b) Plot of the relative (to water) intensities of the 3450 cm^{-1} peak. The relative intensities from the SFG spectra are compared with the product of the relative intensities of the corresponding peaks from the isotropic Raman and IR spectra.

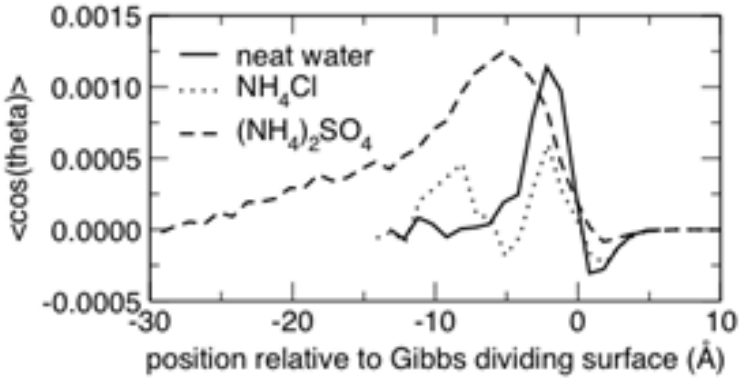

Figure10. Orientation polarizations (see text for details) from MD simulations as functions of position in the slabs relative to the Gibbs dividing surface (defined as the position where the water density is equal to half its bulk value).

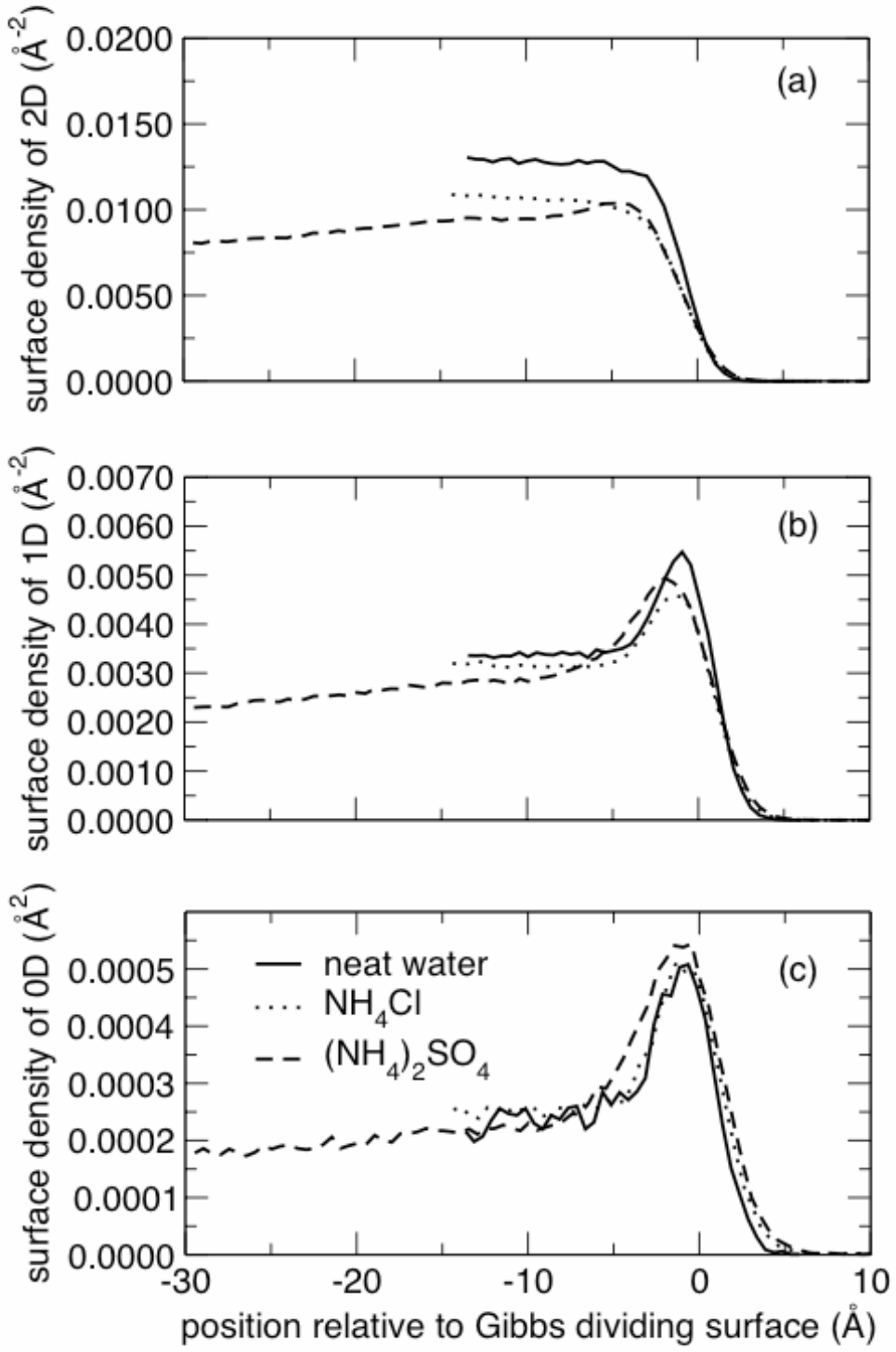

Figure 11. Number of water OH bonds per unit area in water molecules for which: (a) both OH bonds are involved in water-water hydrogen bonds (2D); (b) one OH bond is free and one is involved in a water-water hydrogen bond (1D); both OH bonds are free (0D). The hydrogen bond definition is described in the text.

Table 1. Previously observed NH_4^+ and SO_4^{2-} Raman and IR bands in $(NH_4)_2SO_4.11H_2O$ – adapted from reference 45.

Raman		IR	
Peak Position (cm^{-1})	Assignment	Peak Position (cm^{-1})	Assignment
980	Sulfate symmetric stretch	1103	Sulfate asymmetric stretch
2875	2nd overtone of NH_4^+ umbrella bending	1450	NH_4^+ umbrella bending
3060	Combination band of NH_4^+ umbrella bending and rocking	2890	2nd overtone of NH_4^+ umbrella bending
3115	NH_4^+ symmetric stretch	3060	Combination band of NH_4^+ umbrella bending and rocking
3215	NH_4^+ asymmetric stretch	3230-3480 Very broad, very intense absorption	-

Table 2. Raman Fit Parameters (Gaussian)

	Peak Position (cm^{-1})	Amplitude	FWHM	Area
H_2O	3248.9	6620	243.2	1390540
	3468.4	8724	222.7	1526300
	3628.8	1509	105.9	122730
2M NH_4Cl	2878.7	109.7	89.1	10255.5
	3026.9	439.9	143.7	67291.3
	3248.9	4757.0	243.3	1232330
	3468.4	7439.5	222.5	1762110
	3628.8	714.4	106.2	80841.9
1M Na_2SO_4	3248.9	4707.9	233.0	1167870
	3468.4	6813.2	234.2	1698320
	3628.8	682.6	84.0	61067.4
1M $(NH_4)_2SO_4$	2878.7	107.4	92.6	10574
	3032.1	472.1	159.2	79990
	3248.9	4836.7	243.3	1252760
	3468.4	6450.6	222.5	1527830
	3628.8	781.0	106.2	88312

Table 3. FTIR-ATR Fit Parameters (Voigt)

	Peak Position (cm^{-1})	Amplitude	FWHM	Area	Voigt Shape
H_2O	3214.6	0.30	251.0	95	1.00
	3391.1	0.20	231.3	54	0.00
	3571.3	0.05	152.0	9	0.00
2M NH_4Cl	2897.1	0.03	245.4	8	1.03
	3052.6	0.05	141.6	8	1.00
	3201.6	0.04	114.0	5	1.10
	3214.6	0.30	252.5	76	1.00
	3391.1	0.20	235.8	60	0.00
	3571.3	0.05	142.4	8	0.00
1M Na_2SO_4	3214.6	0.30	254.0	95	1.00
	3391.1	0.23	236.7	58	0.00
	3571.3	0.05	148.9	8	0.00
1M $(NH_4)_2SO_4$	2888.4	0.02	217.9	6	0.79
	3056.9	0.06	163.8	12	1.00
	3195.7	0.03	105.3	3	0.40
	3214.6	0.30	246.5	83	1.00
	3391.1	0.20	238.1	56	0.00
	3571.3	0.05	146.8	8	0.00

Table 4. SFG fit parameters (Lorentzian).

	Peak Position (cm^{-1})	Phase	Amplitude	FWHM	Area
H_2O	3207.9	+	210.1	180.3	601.6
	3444.6	+	137.4	117.6	433.0
	3547.0	+	21.9	78.0	17.3
	3703.1	-	62.4	19.1	627.6
	3748.5	-	58.8	74.9	119.2
2M NH_4Cl	3242.8	+	155.9	158.0	392.5
	3414.9	+	159.0	122.5	555.1
	3547.5	+	21.3	78.7	16.2
	3701.8	-	60.1	19.2	613.5
	3748.5	-	55.2	74.8	106.7
1M Na_2SO_4	3207.3	+	246.9	160.9	956.3
	3444.1	+	158.9	114.1	600.3
	3547.9	+	22.7	78.4	18.5
	3703.2	-	62.4	17.5	686.7
	3748.5	-	58.1	74.9	116.3
1M $(NH_4)_2SO_4$	3218.4	+	267.5	163.5	1103.9
	3441.4	+	188.7	107.4	907.6
	3549.3	+	25.6	78.4	23.4
	3704.9	-	62.4	18.4	653.8
	3749.5	-	59.2	74.2	121.7

Cover Art:

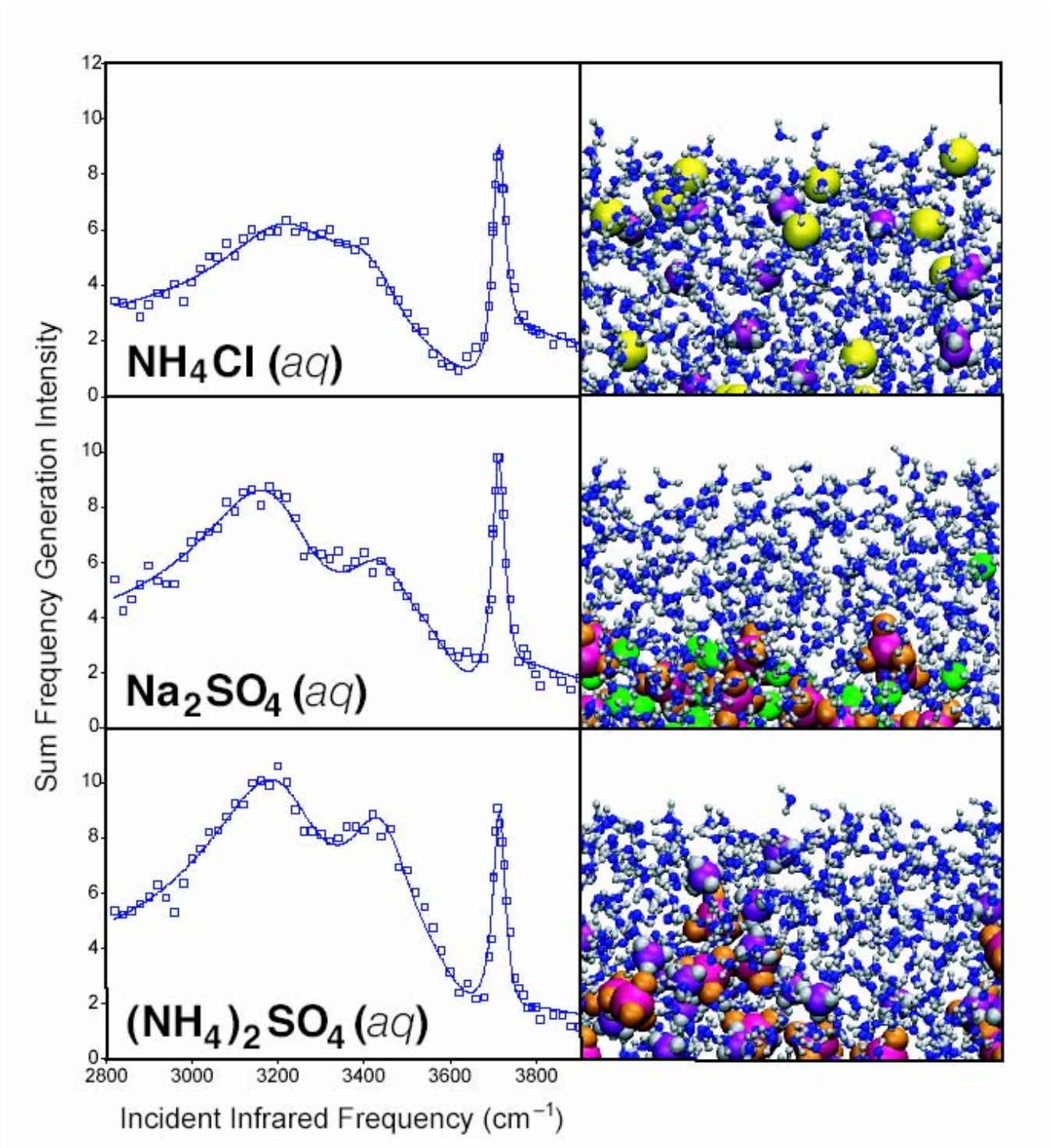

Cover Art suggested caption:

Sulfate dianions are strongly repelled from aqueous surfaces and increase the interfacial thickness.